Contents lists available at http://qu.edu.iq

Al-Qadisiyah Journal for Engineering Sciences

Journal homepage: https://qjes.qu.edu.iq

Mechanical compressive properties of TPU 3D printed with various parameters

Ahmed A. Ameen[1*], Ayad M. Takhakh[1], and Abdalla Abdal-hay[2, 3, 4]

[1]*Mechanical Engineering Department, College of Engineering, Al-Nahrain University, Baghdad 10072, Iraq*
[2]*Faculty of Industry and Energy Technology, Mechatronics Technology Program, New Cairo Technological University, Cairo, Egypt*
[3]*Department of Engineering Materials and Mechanical Design, Faculty of Engineering, South Valley University, Qena 83523, Egypt*
[4]*The University of Queensland, School of Dentistry, Oral Health Centre Herston, 288 Herston Road, Herston, QLD 4006, Australia*

ARTICLE INFO

Article history:
Received 08 April 2024
Received in revised form 11 August 2024
Accepted 03 November 2024

Keywords:
Fused Deposition Modeling
Shape memory polymer
Thermoplastic polyurethane
Printing parameters
Mechanical properties

ABSTRACT

Shape memory polymer (SMP) is a material that has the ability to recover its original shape from a temporary (deformed) shape by applying external stimuli. The smart scaffold based on SMP is used to enhance delivery, load bearing, and tissue defect filling. Therefore, specimens with the structure of the face-centered cubic were produced under various printing conditions to characterize their effects on the mechanical properties. Fused deposition modeling is utilized to construct the specimens of shape memory thermoplastic polyurethane (MM-3520). Printing parameters with different levels were used in specimen fabrication, including layer thicknesses of 0.1, 0.2, and 0.3 mm, printing temperatures of 210, 220, and 230 ° C, and printing speeds of 20, 30, and 40 mm/sec. We performed the microstructural analysis under a microscope to examine the impact of printing factors on lattice structures. Then there is the compression test, which evaluates mechanical properties such as linear elastic stiffness, collapse stress, plateau stiffness, and densification stress. Analyzing the microstructure of the printed specimens exhibits that the specimens with the highest printing temperature, the lowest printing speed, and a thinner printing layer have better layer adhesion and lower porosities. As well, figures and main effect plots revealed that the specimens printed with a layer height of 0.1mm, a printing temperature of 230 ° C, and a printing speed of 20 mm/s had compressive strengths of 0.6129±0.062, 0.6018±0.106, and 0.6082±0.078 MPa, respectively. These are the highest results in terms of strength compared to other levels of parameters.

1. Introduction

The 3D printing is a highly adaptable and groundbreaking technology that allows for the fabrication of complex and personalized objects with unparalleled accuracy [1, 2]. The growing use of shape memory polymers (SMPs) in the medical and scientific fields, coupled with rapid advancement in 3D printing production technology, necessitates the precise modification of the mechanical properties of these objects [3].

Interestingly, 4D printing attracts great attention to SMPs in multi-displines [4]. SMPs have the advantage of lower processing temperatures and costs compared to shape-memory alloys. Moreover, shape-changing functionality in SMPs is better than in shape memory composites [4]. Smart materials such as SMPs can change their shapes and then recover the original shapes after being subjected to external stimuli [5].

* *Corresponding author.*
E-mail address: ahmeda.ameen94@gmail.com (Ahmed Ameen)

https://doi.org/10.30772/qjes.2024.148664.1193
2411-7773/

Nomenclature:

E_i	Linear elastic stiffness (MPa)	σ_d	Densification stress (MPa)
σ_i	Collapse stress (MPa)	E_p	Plateau Stiffness (MPa)

Due to their unique thermo-mechanical properties, SMPs have attracted a lot of interest; therefore, these properties make them suitable for use in flexible electronics, aircraft components, medical instruments, etc. [6]. However, the feasibility of using these types of materials in specific applications is depending directly on the mechanical functionality of the printed structures [5]. Additive manufacturing, commonly referred to called as 3D printing, involves the sequential addition of fused material layers to construct three-dimensional parts [7]. Fused deposition modeling (FDM) is a popular technique among additive manufacturing methods [4]. This method includes 3D objects built by depositing the melted polymer across the nozzle onto the platform, where the computer-aided design data file specifies the construction method, layers, and paths to build such items [4]. As well as, produces various items more efficiently and cost-effective than conventional methods [8]. Generally, FDM procedures use thermoplastic polymers like acrylonitrile butadiene styrene (ABS), thermoplastic polyurethane (TPU), and polylactic acid (PLA) [9]. The printing parameters used during the fabrication process, for example, printing temperature, printing speed, infill density, and layer thickness, directly affect The mechanical properties of 3D-printed SMPs [10]. Therefore, it is important to regulate and match the factors of 3D printing with the resulting mechanical characteristics of the polymers to improve practical applications [11]. Slight alterations in these parameters could have a significant impact on properties of an object, such as elasticity, tensile strength, and shape memory characteristics [10]. For example, Villacres et al. printed the TPU MM-4520 specimens at various angles and infill densities [12]. The delamination of neighboring layers during stress application may be the cause of the observed decrease in tensile strength for printing angles greater than zero [12]. The modulus of elasticity is directly proportional to the infill density, resulting in higher strength [12]. In addition, Liu et al. [13] used patterns of linear with a 0° angle and rectilinear with ±45° and ±60° angles to produce tensile specimens. The tensile strength would decrease as the inclination angle increased, due to a lower adhesive strength between filaments compared to that along printed fibers [13]. While Buj-Corral et al. investigated the effect of increasing printing speed on the surface roughness and dimensional accuracy of the SMP products [14]. Faster printing speeds cause the temperature of the extruded polymer to decrease at a faster rate, resulting in irregular material extrusion and, therefore, higher surface roughness and lower dimensional accuracy [14]. Whereas Rosales et al. used Dia PLEX and TECO flex with different printing layers. They conducted research on how changes in layer thickness, printing temperature, and printing speed affected the Young's modulus [15]. The following factors make Young's modulus better: higher printing temperatures help the layers stick together better; thicker layers make the cross-sectional area of the fibers bigger and rid of more flaws; and slower printing speeds make the solidification more even and lower the residual stresses [15]. Yao et al. found that the tensile strength of the PLA specimens decreased as the layer thickness proportion increased [16]. This was because the deposited filament became more compact in the thinner layer specimens [16]. Singh et al. conducted research to study the mechanical properties of SMPs by using infill densities of 20%, 60%, and 100% [17]. They fabricated samples from three distinct materials: PolyFlex, ABS, and a blend of PolyFlex and ABS (70/30 vol%). The research findings suggest that increasing infill density leads to a corresponding increase in tensile strength, break strength, peak strength, break load, and peak load. The higher number of fibers available to withstand the applied loads and the denser infill provide more material to resist deformation and failure under load [10, 17]. In the research by Chalgham et al. utilized the FDM technique with a PLA filament [18]. The operating temperatures to fabricate specimens were 190 and 230 °C.

This study revealed that the enhanced interconnection between the deposited layers led to a slight 3% increase in bending strength. Our study seeks to investigate and describe the correlation between 3D printing parameters and the mechanical properties of the SMP. The study's results will offer a practical perspective, potentially leading to the customization of SMP applications' properties. We used SMP thermoplastic polyurethane MM-3520 to achieve this. Cellular cubical specimens were printed by varying three printing factors: printing speed (20, 30, and 40 mm/s), printing temperature (210, 220, and 230 °C), and layer thickness (0.1, 0.2, and 0.3 mm). During the printing process, these parameters were adjusted and controlled carefully. These parameters were adjusted and controlled carefully during the printing process. The compression test was executed to evaluate the impact of manufacturing factors on the mechanical properties. This research shows a feasible way to analyze the mechanical properties of a shape memory bone scaffold with a microstructure lattice. This has a lot of potential for using in the applications of bone defect repair.

2. Experimental methods

2.1. Material

In this investigation, we used thermoplastic polyurethane (MM-3520, SMP Technologies, Inc., Japan) as a filament with 1.75 mm average cross section diameter to create the cubical cellular specimens. The glass transition temperature (T_g) of TPU MM-3520 is 35 ° C; therefore, TPU can recover its original shape at this temperature. The T_g (35 ° C) enables us to build bone scaffolds because it responds to body temperature as stimuli. This type of SMP is efficient enough to be used on FDM 3D printers [1].

2.2. Production

SolidWorks software (SolidWorks Corp., Dassault Systems, 2023) is CAD software that is used to design specimens. After that, the design was exported to slicing software such as (Ulti Maker Cura 5.4.0). This software can concert 3D models into G-code, which is a language that 3D printers can comprehend. This ensures that the printer is equipped with the necessary instructions to construct the model in a sequential manner, layer by layer. Additionally, it allows users to modify other parameters, including layer height, print speed, printing temperature, printing angle, printing orientation, and infill density. A desktop fused deposition modeling (FDM) 3D printer (ANYCUBIC MEGA Pro) with a nozzle size of 0.4 mm was employed to fabricate the specimens. The printing parameters that specified to produce the specimens are listed in Table 1.

The Design of Experiment (DOE) by Taguchi method is being implemented in Minitab software to study the impact of fabrication parameters on the specimen material characteristics. According to prior research, the following variables directly influence the quality of the printed body: nozzle temperature, which refers to the filament temperature inside the nozzle and during deposition [19]; printing velocity, which pertains to the speed of nozzle motion over the printing bed during deposition [20]; and layer thickness, this parameter means the height of deposited material at each level of printing process [21].

Table 1. Fabrication parameters for 3D printing of scaffold test specimens.

Printing Parameters (Unit)	Values
Extrusion temperature (° C)	210, 220 and 230
Bed temperature (° C)	45
Nozzle diameter (mm)	0.4
Layer thickness (mm)	0.1, 0.2 and 0.3
Printing speed (mm/s)	20, 30 and 40
Infill pattern	Straight line

Three levels were specified for each factor. The levels of the factors were determined according to Bruère et al. [22] and Brancewicz-Steinmetz et al. [23]. Table 2 presents the factors and their levels in each run that derived from a DOE for SMP. Each set of samples included altering certain printing settings while keeping the others constant. As an example, when modifying the height of the printing layers (0.1, 0.2, and 0.3 mm), the printing speed and printing temperature remain constant at 30 mm/s and 220 °C respectively. The sets produced at different printing temperatures (210, 220, and 230 °C) maintained a constant printing speed of 30 mm/s and a layer thickness of 0.2 mm. This is also applied to altered printing speed (20, 30, and 40 mm/s); they were manufactured with a printing temperature of 220 ° C and a layer height of 0.1 mm.

Table2. DOE runs for TPU

RUN	Layer Thickness (mm)	Printing Temperature (° C)	Printing Speed (mm/sec)
1	0.1	220	30
2	0.2	220	30
3	0.3	220	30
4	0.2	210	30
5	0.2	230	30
6	0.2	220	20
7	0.2	220	40

2.3. Microstructure analysis

The microstructures of the extruded filament and printed items were examined using an optical microscope (Olympus BX60M) at a magnification of x5.

2.4. Mechanical properties

The mechanical characteristics of the rectangular scaffold samples, measuring 16x16x16 mm as shown in Fig. 1, were assessed using an Instron Universal testing machine (Test metric, M500-25kN). The force was exerted until the sample was compressed to around 50% of its initial length, using a crosshead speed of 1.3 mm/min. According to the specifications stated in ASTM standard D695-96, three scaffold samples were used in each group, all printed using identical settings. This was done to calculate an average value. The design of the scaffolds should typically mimic the porosity of bone tissue, which is around 70% [24, 25]. The dimensions of the pores on the sides of the sample, as seen in Fig. 2, are 1 mm in height and 2.24 mm in width. On the other hand, the pores at the top and bottom of the specimen have dimensions of 2.24 mm in height and 2.24 mm in width. The scaffolds were fabricated for each condition using horizontal printing, which resulted in improved Fiber alignment and bonding compared to other printing planes [26].

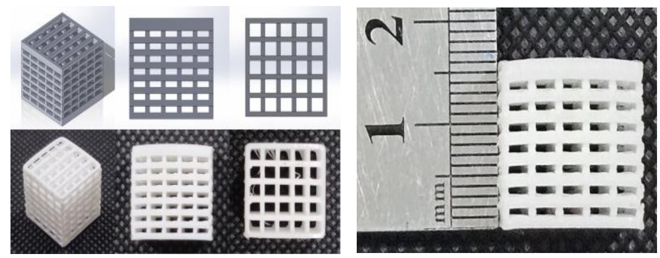

(a) (b)

Figure 1. (a) Design of the sample from different views and (b) dimensions of the sample

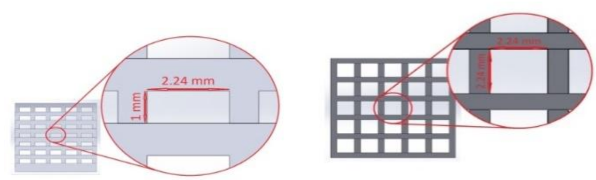

(a) (b)

Figure 2. (a) Dimensions of the pores at the sides of the sample and (b) Dimensions of the pores at the top and bottom of sample.

2.5. Statistical Analysis

The data of mechanical properties (elastic stiffness, collapse stress, plateau stiffness, and densification stress) were provided as the mean ± standard deviation (SD). Statistical analysis was conducted using the one-way analysis of variances (ANOVA) and post hoc Tukey honestly significant difference (HSD) with statistically significant with 95% confidence (P-value < 0.05). This analysis was performed in Origin Lab Pro 2024 software.

3. Results and discussion

3.1. Microstructure analysis

3.1.1. Layer thickness parameter

The layer height influences the microstructure of the TPU-printed biomaterial. Thinner layers, such as 0.1 mm, exhibit over-compaction, the highest compression ratio to the extruded fibers during printing [27]. This results in clear mixing between adjacent layers of extruded fiber, increasing the bonding area between the layers. Increasing the layer height to 0.2 mm has reduced the impact of the compression ratio, weakening the mixing zone [28], as seen in the comparison between Figs. 3 (a and b). The specimen with a layer thickness of 0.3 mm exhibits reduced connection area, resulting in a groove between the printed fibres, seen inFig. 3 (c), and the region within the red circle in Figs. 4 (a and b).

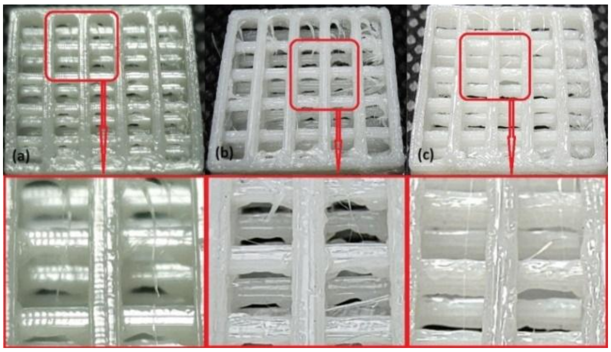

Figure 3. Effect of layer thickness on the structure of the specimens (a) 0.1mm layer thickness, (b) 0.2mm layer thickness, and (c) 0.3mm layer thickness

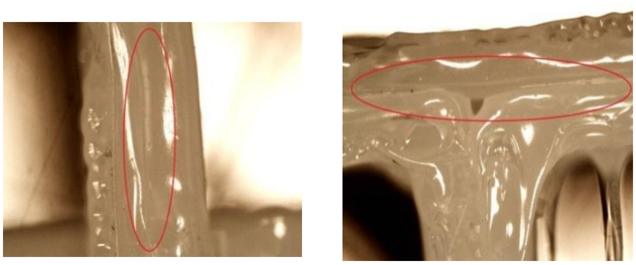

(a) (b)

Figure 4. Effect of 0.3 mm layer thickness on the structure (a) strut area and (b) join area.

In addition, Figs. 5 (a and b) shows that a thinner layer thickness results in a broader contact area and fewer porosities. A decrease in layer height results in a narrower gap between layers, which promotes the mechanisms of bonding and interdiffusion due to an elevated compression ratio [27]. A layer height of 0.3 mm leads to significant porosity, primarily found in the interlaminar zone as seen in Fig. 5 (b).

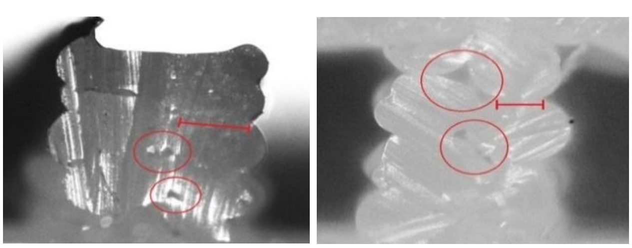

(a) (b)

Figure 5. Cross-sectional view of contact area and porosities in (a) 0.2mm and (b) 0.3mm specimens

3.1.2. Printing Temperature Parameter

Increasing the temperature enhances the flow and reduces the viscosity of the polymer [29], resulting in smoother surfaces when comparing specimens printed at various temperatures (210, 220, and 230 ° C) as seen in Figs. 3 (b) and 6 (a and b). Low temperature (210 ° C in Fig. 6 (a)) could affect the smooth extrusion of TPU filament through the nozzle. This would lead to irregular flow, blockages, flaws, and blemishes on the surface. Specimens printed at 220 ° C revealed smoother surfaces and fewer flaws due to the increased flowability and reduced viscosity of the polymer at this temperature [29]. The presence of bubbles in the samples at 230 ° C will impact the surface quality findings. This flaw becomes apparent at high temperatures as the material becomes almost liquid as it enters the extruder nozzle, but it is essentially non-existent at lower temperatures. Other authors suggest that greater temperatures lead to a reduction in viscosity. As the polymer moves across the nozzle, friction against the walls creates turbulence that aids in air intake [28-30].

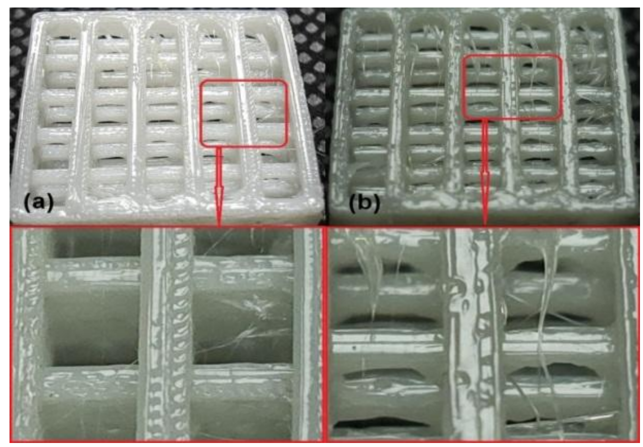

Figure 6. Illustration the top view texture of the printed specimens with (a) 210 ° C and (b) 230 ° C.

The comparison of the cross-sectional views in Figs.5 (a) and 7 shows that at high temperatures, the polymer becomes almost liquid before reaching the extruder nozzle [31], causing the width of the extruded filament to expand. Consequently, the contact area between the two adjacent fibers also increases. An increase in extruder temperature leads to a higher part density due to a drop in the viscosity of the SMP material, allowing it to flow more smoothly through the nozzle [31]. This results in an increased amount of material being used to create the model. Fig. 7 (lower temperature) shows significant gaps between layers and holes between infill filaments within the same layer. Figure 5a shows fewer voids at higher temperatures.

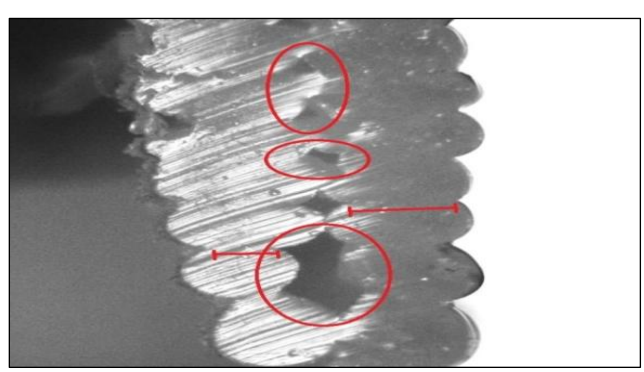

Figure 7. Cross-sectional view of the specimen printed with 210 ° C.

3.1.3. Printing Speed Parameter

Our investigation verified that the printing speed impacts the deposition of filaments, influencing print quality. Irregularities arose in the curved sections, breadth, and connections of adjacent filaments because of the inadequate coordination between the printing speed and extrusion speed. The image analysis findings indicated that the deposition of SMP filaments was successful at printing rates of 20, 30, and 40 mm/s, as shown in Fig. 3 (b) and Figs. 8 (a and b). At increased velocities, the extruded filaments experienced deformation at the connecting areas between two fibers during deposition. The breadth of the filaments within a layer was inconsistent and variable, as seen in Fig. 8 (b). The interface between two neigh boring layers is more distinct when printing rates are slower, namely around 20 and 30 mm/s as shown in Figs. 3 (b) and 8 (a). Higher printing rates caused issues with filament feeding into the extrusion nozzle owing to the filament's lack of stiffness, leading to interruptions in the extrusion process [30].

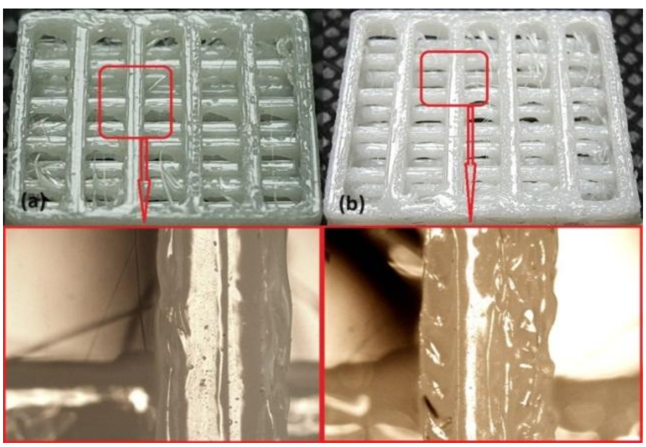

Figure 8. Top view the texture of samples printed with (a) 20 mm/s and (b) 40 mm/s.

Another discovery has been made that temperature and holding time significantly impact bond formation [19]. Additionally, the cavities occur within the red circle in Fig. 9 when the TPU infill filaments elongate at higher printing speeds. The density of the specimen reduces as the scanning speed of the nozzle increases. Insufficient material extrusion due to the high scanning speed can lead to the formation of voids [30], as seen in Fig. 9.

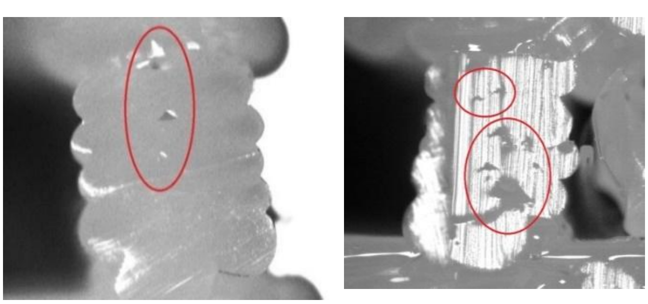

(a) (b)

Figure 9. Cross-sectional view of specimens printed with (a) 20 mm/s and (b) 40 mm/s

3.2. Mechanical properties

In addition to promoting bone tissue development by filling bone deficiencies, the scaffolds must also possess sufficient structural integrity to resist the forces exerted during regular walking. The ground exerts a response force on the foot when walking that is 1.5 times the individual's body weight. The femur has a diameter ranging from 6 to 10 cm. Typically, the narrowest part of the femur for an adult weighing 60 kg is around 6 cm. Thus, when a scaffold is placed in this location, it will endure a stress of 0.21 MPa. The scaffolds will meet the mechanical criterion if the yield strength exceeds 0.252 MPa, assuming a safety factor of 1.2 [32]. To examine the compressive characteristics, compression tests were carried out at room temperature using the settings specified in section (2.3). Figure 10 shows the specimen before and after the compression test.

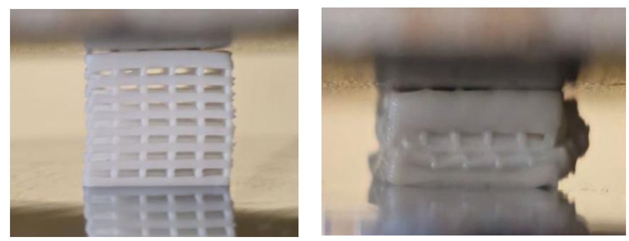

(a) (b)

Figure 10. (a) specimen before compression and (b) specimen after

Figure 11 demonstrates the occurrence of elastoplastic deformation under compression [35].

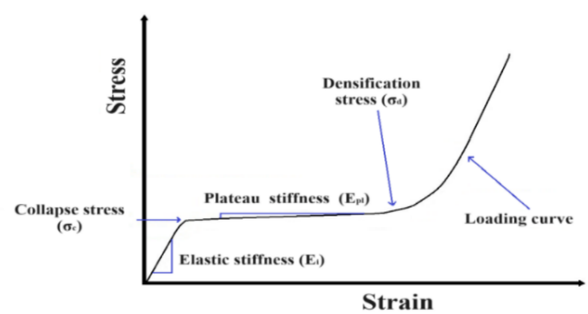

Figure 11. Stress-strain curve for the elastic material in compression with definition of material characteristics.

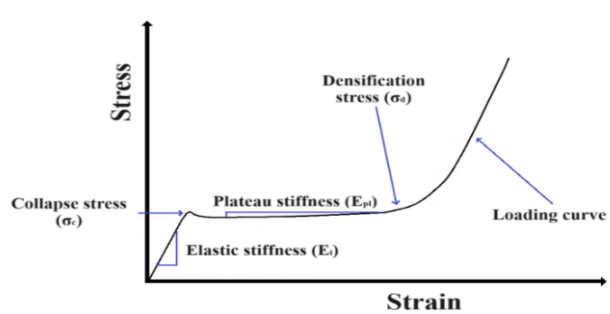

Figure 12. Stress-strain curve for the elastic-plastic material in compression with definition of material characteristics.

Gibson et al. [33] and De Vries [34] described the material characteristics and identified them from the stress-strain data, as shown in Figs. 11 and 12. Figure 11 represents the elastomeric polymer behaviour, while Figure 12 is specific to the elasto-plastic material pattern. The important material properties of flexible materials can be defined as follows: The first stage corresponds to a linear deformation caused by the mechanical characteristics of the material being tested and the geometric stiffness of the individual cells in the specimen (which represents the average stiffness in the linear elastic area, denoted as E_i) [33-36]. The subsequent phase of deformation is triggered by the destabilization and the onset of bending and buckling mechanisms within one of the structural layers (which encompasses the average collapse stress (σ_c), defined as the stress at which cells in the polymer structure begin to collapse under compression) [33-37].Figures 11 and 12 exhibit a prolonged plateau, which signifies an additional stage of deformation. The occurrence of this phenomenon is attributed to the steady development of bending and buckling processes within certain layers of the structure. These layers exhibit plateau stiffness (E_{pl}), which refers to an area where the material maintains a relatively constant stress despite an increase in strain [35, 36]. This phenomenon takes place after the early phase of linear elasticity and before any substantial deformation or failure. Throughout the plateau phase, the material experiences processes such as yielding or buckling, resulting in a consistent amount of stress. The rigidity throughout this period is likely to be rather consistent, leading to a plateau in the curve. The stiffness of the plateau reflects the material's capacity to endure deformation while maintaining a steady load [33-36]. The last phase is densification stress (σ_d), characterized by a significant increase in the magnitude of the stress, is associated with the complete failure of all arrays inside the specimen and the ultimate compaction of the structure [33-36]. An analysis of variances (ANOVAs) was performed to evaluate the values of E_i, σ_c, E_{pl}, and σ_d for various printing parameter settings and they were statistically significant with 95% confidence (P-value < 0.05). The results of the one-way ANOVAs and post hoc Tukey honestly significant difference (HSD) tests are shown the following figures.

3.2.1. Layer Thickness Parameter

Figures 14 and 16 show the collapse stress (σ_c) of the thickness of three scaffolds as the layer varies (0.1, 0.2, and 0.3 mm) while keeping other parameters constant.

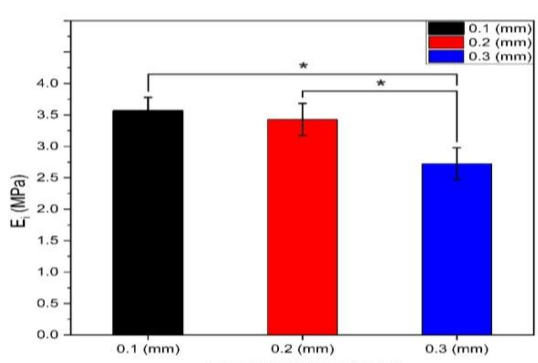

Figure 13. Elastic stiffness of samples printed with layer thicknesses of (0.1, 0.2 and 0.3 mm).Note: An asterisk indicates the digits of statistically significant difference (*=p < 0.05, **= p < 0.01, ***= p < 0.001, and ****= p < 0.0001)

The samples generated with layer thicknesses of 0.1, 0.2-, and 0.3-mm exhibit collapse stresses of 0.6129±0.062, 0.5933±0.078, and 0.4628±0.08 MPa respectively. Decreasing the thickness of the layers in 3D printed TPU (Thermoplastic Polyurethane) may greatly improve the E_i and σ_c of the final product. When the layer height from 0.3 mm to 0.1 mm, the adhesion between each layer and the one below it improves, resulting in improved interlayer bonding. The enhanced adhesion reduces the risk of separation and improves the overall strength of the printed item. In addition, thinner layers result in a more polished surface, fewer voids, and increased sample density. This, in turn, reduces the risk of stress concentration spots that might potentially undermine the compressive strength [38-40]. Also, the findings in Section 3.1 demonstrate that the compression ratio, reflecting the pressure on the filament during printing, may enhance the mechanical and microstructural characteristics by affecting the bonding process between the printed layers [29].

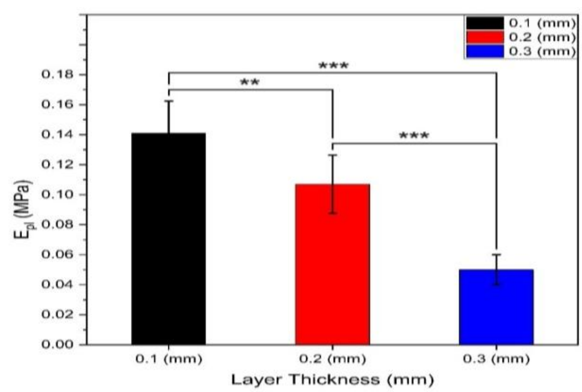

Figure 14. Collapse stress of samples printed with layer thickness (0.1, 0.2 and 0.3 mm).

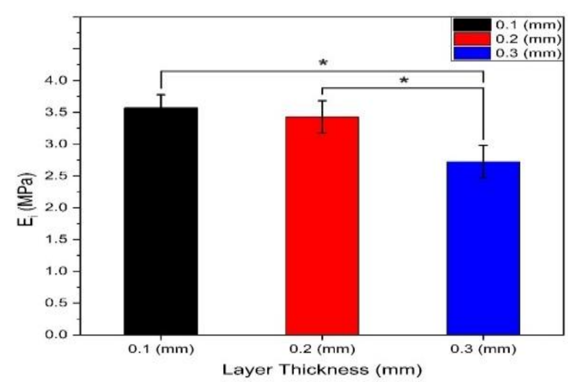

Figure 15. Plateau stiffness of samples printed with layer thicknesses of (0.1, 0.2 and 0.3 mm).

Figure 17 shows the mechanical property indicators and stress-strain curves for three distinct line curvatures of the lattice structures that were printed with different layer depths (0.1, 0.2, and 0.3 mm). These three lines exhibit the same pattern of elastoplastic features (E_i, σ_c, E_{pl}, and σ_d), but they vary in their values and the times they occur. Reducing the layer height increases the linear elastic stiffness (E_i) and collapse stress (σ_c) as shown in Figs. 13 and 14. This is because thinner layer thicknesses generally result in improved layer adhesion and greater material density, which in turn contribute to a more rigid structure [38, 41, 42]. Notably, the stage that includes the plateau stiffness (E_{pl}) for 0.2 mm specimens has a greater stress value in comparison with the other stages as shown in Fig. 17. The trend line of 0.1 mm descends below the curve of 0.2 mm specimens before the densification stage. Furthermore, the characteristic known as E_{pl} in the 0.3 mm specimens exhibits the smallest quantity compared to the 0.2 and0.1 mm specimens.

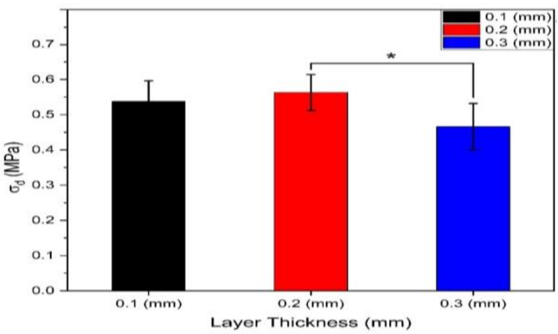

Figure 16. Densification stress of samples printed with layer thicknesses of (0.1, 0.2 and 0.3 mm).

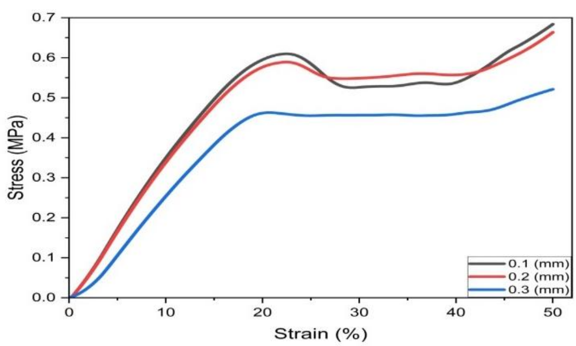

Figure 17. Stress-strain curves of samples printed with layer thicknesses of (0.1, 0.2 and 0.3 mm).

3.2.2 Printing Temperature Parameter

Increasing the printing temperature from 210 to 230 ° C for 3D-printed TPU would enhance its compressive strength. TPU is a thermoplastic substance that experiences changes in its physical state throughout the printing process. The increased temperature improves the polymer's ability to flow and decreases its viscosity, resulting in increased contact area and improved interlayer adhesion.

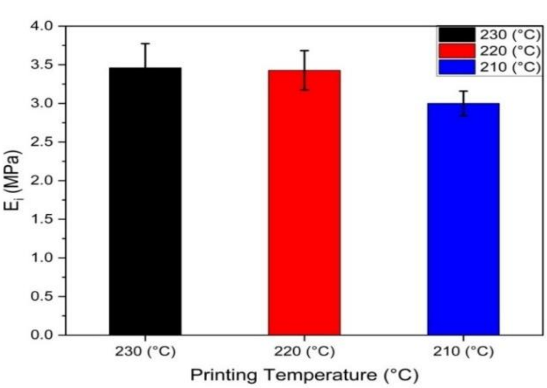

Figure 18. Elastic stiffness of samples printed with printing temperatures of (210, 220 and 230 ° C).

The enhanced adhesion between layers leads to a stronger and more unified structure, thus raising the elastic stiffness and the collapse stress of the product [40, 43, 44]. Furthermore, Lower heating temperatures cause incomplete melting of the crystalline areas, while higher printing temperatures provide more energy and allow extra heating time for SMP TPU MM-3520. Therefore, increased temperature enhances the crystallinity, improving thereby the mechanical characteristics of the product [28].

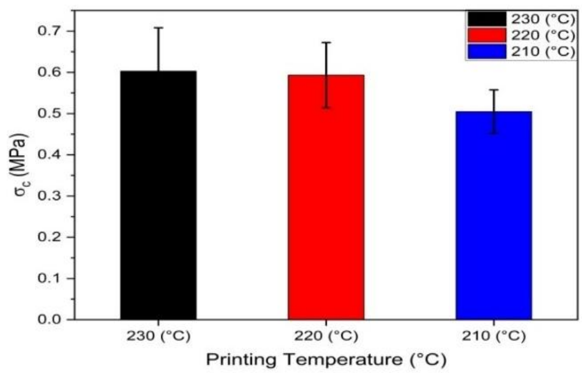

Figure 19. Collapse stress of samples printed with printing temperatures of (210, 220 and 230 ° C).

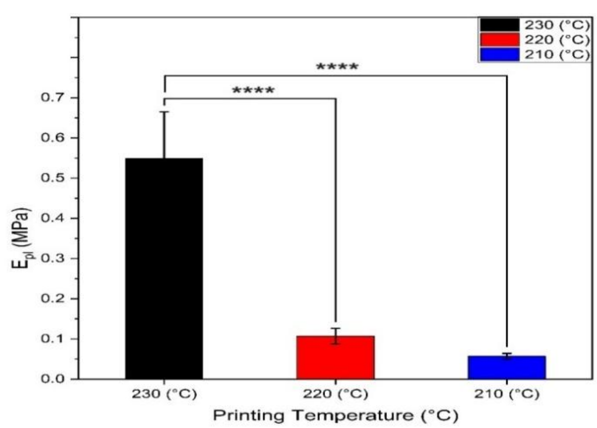

Figure 20. Plateau stiffness of samples printed with printing temperatures of (210, 220 and 230 ° C).

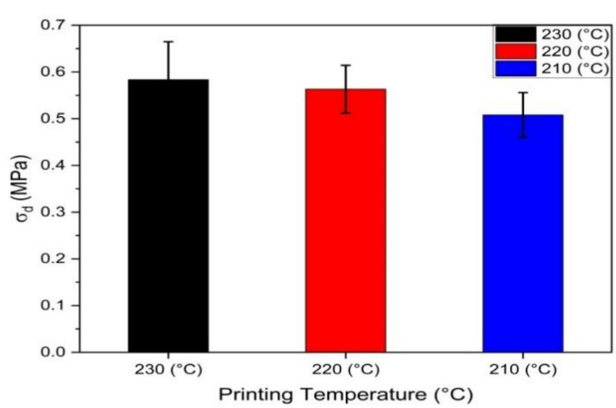

Figure 21. Densification stress of samples printed with printing temperatures of (210, 220 and 230 ° C).

Figure 22 illustrates the stress-strain curves and mechanical property indicators for three-line curvatures for specimens with the same lattice structures and printed at 210, 220, and 230 ° C. The image clearly illustrates the distinct elastoplastic features of these three curve lines, although their values and times of occurrence differed. Modifying the printing temperature of TPU (thermoplastic polyurethane) could significantly affect the mechanical characteristics of the printed material. Generally, raising the printing temperature may improve the linear elastic stiffness (E_i) shown in the stress-strain curve as shown in Fig. 18. The main reason for this is the higher temperature, which enhances the bonding between layers and the alignment of molecules, leading to a stiffer structure. Therefore, a higher printing temperature can result in elevated collapse stress (σ_c) as shown in Fig. 19, due to the increased resistance to deformation and possibly a steeper slope in the linear elastic zone [38, 40, 42]. Furthermore, the region that exhibits the plateau stiffness (E_{pl}) for samples at 220 ° C has a greater value of stress compared to the other stages and reaches the densification stage earlier as shown in Fig. 22. However, this point on the trend line, which is at a temperature of 230 ° C, is located below the curve at 220 ° C before the stage of densification. The 210 ° C line has the lowest values compared to the other parameters (230 and 220 ° C).

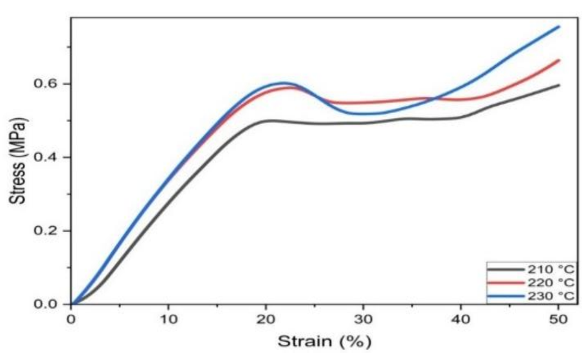

Figure 22. Stress-strain curves of samples printed with printing temperatures of (210, 220 and 230 °C).

3.2.3 Printing speed parameter

Lowering the printing velocity from 40 to 20 mm/s during the 3D printing process of TPU could significantly improve the linear elastic stiffness and collapse stress, as shown in Figs. 23 and 24. Reduced printing rates provide improved heat dissipation and enhanced layer adhesion.

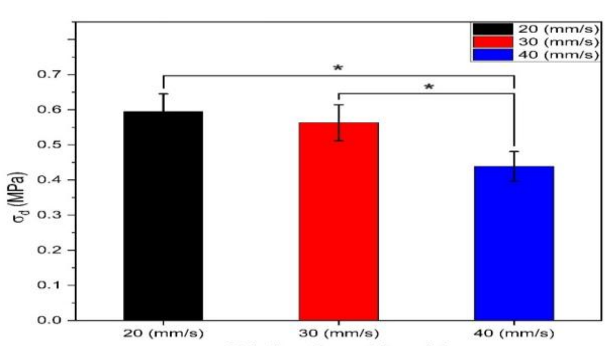

Figure 23. Elastic stiffness of samples printed with printing speeds of (20, 30 and 40 mm/s).

Reducing the speed of the printing process allows each layer to have a longer duration for bonding with the previous layer, resulting in the formation of stronger connections between layers as illustrated in previous Section (3.1). The improved bonding is essential for strengthening the entire structure of the 3D-printed TPU item, especially in situations where compressive strength is of utmost importance [39, 40, 45, 46]. Furthermore, higher printing rates lead to decreased mechanical characteristics due to a shorter forming period, which reduces the crystallinity of TPU. Each successive layer will be placed on the preceding layer during printing and solidifies the liquid TPU. Insufficient contact time between layers and infill filaments reduces the time for polymer chains to disperse and crystallize, resulting in better bonding of the polymer infill filaments [28].

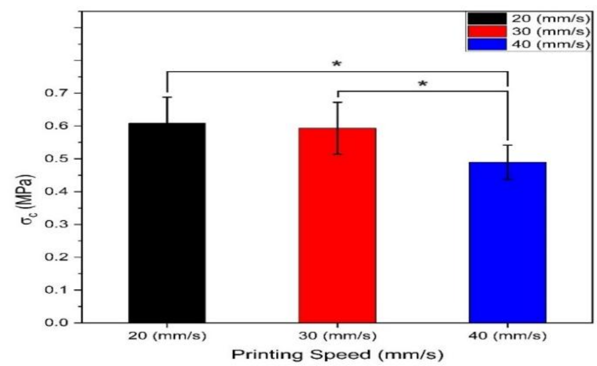

Figure 24. Collapse stress of samples printed with printing speeds of (20, 30 and 40 mm/s).

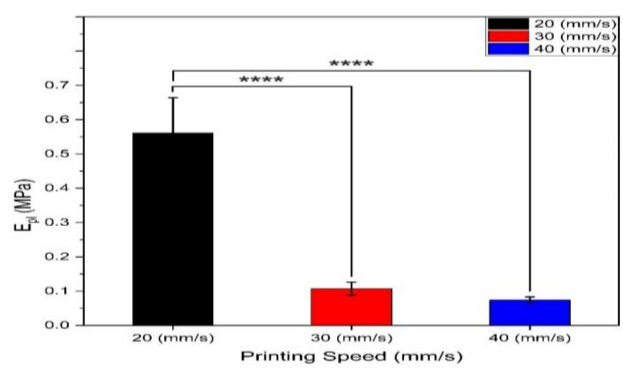

Figure 25. Plateau stiffness of samples printed with printing speeds of (20, 30 and 40 mm/s).

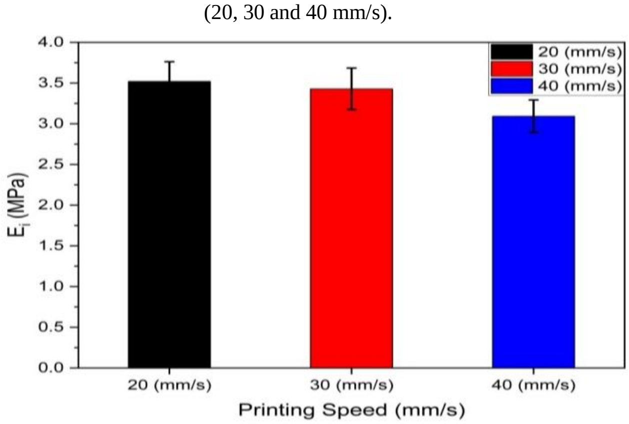

Figure 26. Densification stress of samples printed with printing speeds of (20, 30 and 40 mm/s).

Figure 27 demonstrates the stress-strain curves and mechanical properties for three distinct line curvatures of specimens printed with varying layer thicknesses (20, 30, 40 mm/s). Typically, the stress-strain curve for these values exhibits an elastoplastic behavior. By adjusting the printing speed of this polymer, one may expect changes in both the linear elastic stiffness (E_i) and collapse stress (σ_c) in the stress-strain curve. Reducing the printing speed may enhance bonding between layers and promote a more orderly arrangement of molecules, which may lead to higher linear elastic stiffness. The reason for this is that a reduced printing speed facilitates enhanced interlayer adhesion and provides an additional opportunity for the polymer to undergo cooling and solidification. Hence, the increased linear elastic stiffness might potentially enhance the collapse stress by providing stronger resistance to deformation in the polymer [13, 38, 40]. Furthermore, when the printing speed is set at 30 mm/s, the structure experiences a higher stress value in the E_{pl} area compared to other rates. The stress for samples with a speed of 20 mm/s reaches the densification phase early.

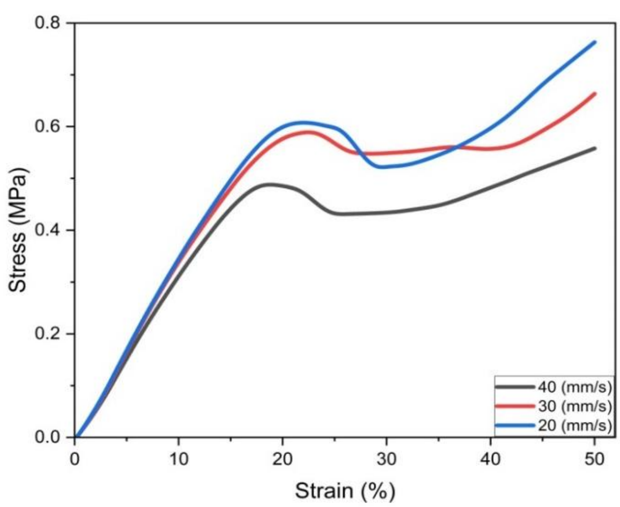

Figure 27. Stress-strain curves of samples printed with printing speeds of (20, 30 and 40 mm/s).

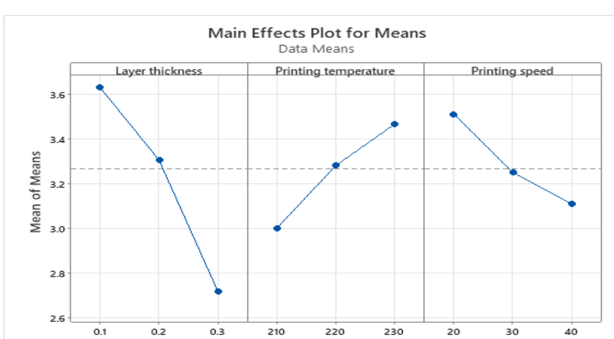

Figure 28. DOE Main effect plot for elastic stiffness

Figures 13, 18, and 23 include elastic stiffness for specimens manufactured with various layer thicknesses, printing temperatures, and printing speeds, respectively. It is generally noted that there is no significant difference between the values of the 0.1and 0.2 mm specimens. This applies also to the 230 and 220 °C specimens in figure 18, as well as the elastic stiffness of the 20 and 30 mm/sec specimens. Similarly, the values of collapse stress in the specimens with parameters (0.1 mm, 230 °C, and 20 mm/sec) do not significantly differ from the (0.2 mm, 220 °C, and 30 mm/sec) specimens, as shown in Figs. 14, 19, and 24. Figure 28 shows the DOE main effects plot for TPU elastic stiffness as a response. It includes an increase in the elastic stiffness value by lowering the layer thickness and printing speeds, as well as increasing the printing temperature. On the other hand, observation reveals that layer thickness primarily influences E_i, with temperature and velocity following closely behind. Figure 29 illustrates the DOE main effects plot for the collapse response. It includes the fact that higher printing temperatures, slower printing speeds, and thinner layer thickness cause greater collapse stress values. This also revealed that layer height would cause the highest impact on the collapse stress; the printing speed was in the second place, and the printing temperature had the lowest one.

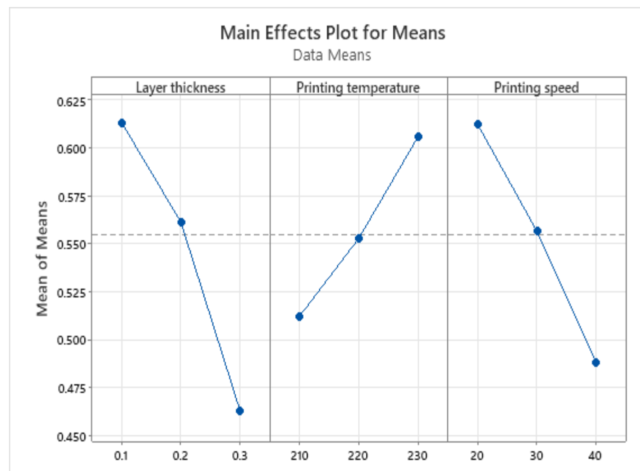

Figure 29. DOE Main effect plot for collapse stress

The plateau stiffness refers to a stage in which the material maintains a consistent stress level despite an increase in strain. It might happen because of the phenomena of buckling and yielding. A higher magnitude of stress in the Tables plateau area means that the object can withstand greater compressive loads during continuous deformation [35, 36]. The samples were built using parameters of 220 ° C nozzle temperature, 0.2 mm layer height, and 30 mm/s printing speed. These parameters would cause the highest stress level in the plateau zone of the stress-strain curve among the other sets of samples. The status of the material confirms its ability to resist compression loads while maintaining its structure despite extreme stress. It also indicates the improvement of the material's strength and resilience during the application of the loads. Additionally, this signifies that the cells of the lattice own a powerful mechanism of energy absorption, which in turn absorbs and spreads compression stresses without exposing them to complete failure [35, 42, 47]. In Figs. 16, 21, and 26, a clear drop is shown in the stress values of the plateau region for the printed structures by using a printing temperature of 230 °C, a printing speed of 20 mm/s, and a layer thickness of 0.1 mm. It might happen due to failure, deformation, yielding, or collapse in the struts (the linkers that connect the components of the sample together). As a consequence, the capacity of the material to withstand further loads has decreased [35]. Another reason is the appearance of plastic deformation (shape change without immediate rise in stress) within the struts. The continuous load might cause further plastic deformation [37]. In addition, the drop in the plateau region stress of the cellular lattice could result from a localized breakdown within these structures. This may include the fracturing or malfunction of individual cells or struts, resulting in a decrease in overall ability to sustain loads [36]. In general, the densification stress (σ_d) as shown in Figs. 15, 20, and 25 is heightened by increasing the printing temperature, as well as by reducing the layer thickness and the printing speed because these factors result in the creation of a stiffer material [35]. Finally, the stress-strain data of the 3D printed TPU MM-3520 in Figs. 16, 21, and 26 clearly demonstrate an elastoplastic pattern [33-36].

3.3. Limitations

Using high printing ranges can affect printing quality and surface roughness. It can also lead to dimensional inaccuracies, affecting the bone scaffold's fit and functionality. Secondly, a specific nozzle diameter restricts the layer height within a specific range; consequently, FDM printing faces constraints in achieving the very fine resolution, which hinders the development of complex and porous structures necessary for the bone scaffold. Finally, the SMP requires accurate temperature control to preserve shape memory characteristics. The inconsistent or high temperatures during the printing operation can cause degradation or undesirable interactions in the material, which can then affect its functionality.

4. Conclusion

The findings of this research indicate that the printing factors, including layer thickness, printing temperature, and printing speed, have a substantial impact on the compression behavior of 3D-printed TPU. The strength and stiffness of the 3D printed item generally increase as the layer thickness and printing speed decrease as well as the printing temperature increases. Modifying these parameters resulted in comparable stress-strain curves, exhibiting an elastoplastic pattern, for every sample set. However, pattern properties such as linear elastic stiffness, collapse stress, plateau stiffness, and densification stress varied, regardless of the infill design or infill percentage. Although samples produced at a speed of 20 mm/s, with a layer thickness of 0.1mm, and at a temperature of 230 ° C exhibit increased stiffness and strength under compression, these parameters may not be considered as optimal. However, considering the stress distribution and energy absorption of the sample. produced, the authors suggest that the results obtained from printing specimens using parameters (0.2 mm - 220 ° C - 30 mm/s) should be used for future improvement of 3D-printed scaffolds in specific applications. This is because the E_i and σ_c values of these specimens are not significantly different from the highest magnitudes obtained from (0.1 mm - 230 ° C - 20 mm/s) E_i and σ_c. Simultaneously, they can endure elevated and constant stress levels for longer time in the plateau area than the others. Producers and 3D printing enthusiasts have access to a wide range of infill patterns and settings through different slicing tools. This research examined a limited number of factors for the same specimen design, which may not include the most suitable features for certain applications. These findings provide a valuable foundation for future exploration of the impact of various printing settings on the performance of 3D-printed bone scaffold designs.

Authors' contribution

All authors contributed equally to the preparation of this article.

Declaration of competing interest

The authors declare no conflicts of interest.

Funding source

This study did not receive specific funds.

Data availability

The data that support the findings of this study are available from the corresponding author upon reasonable request.

REFERENCE

[1] Pieriet al., *Printing Parameters of Fused Filament Fabrication Affect Key Properties of Four-Dimensional Printed Shape-Memory Polymers.* 3D Printing and Additive Manufacturing, 2023. **10**(2): p. 279-288. https://doi.org/10.1089/3dp.2021.0072

[2] Kafle et al., *3D/4D Printing of polymers: Fused deposition modelling (FDM), selective laser sintering (SLS), and stereolithography (SLA).* Polymers, 2021. **13**(18): p. 3101. https://doi.org/10.3390/polym13183101

[3] Sheoran, A.J. and H. Kumar, *Fused Deposition modeling process parameters optimization and effect on mechanical properties and part quality: Review and reflection on present research.* Materials Today: Proceedings, 2020. **21**: p. 1659-1672. https://doi.org/10.1016/j.matpr.2019.11.296

[4] Valvez et al., *Fused filament fabrication-4d-printed shape memory polymers: A review, Polymers (Basel) 13 (2021) 1–25.* https://doi.org/10.3390/polym13050701

[5] Zhao et al., *Research progress of shape memory polymer and 4D printing in biomedical application.* Advanced Healthcare Materials, 2023. **12**(16): p. 2201975. https://doi.org/10.1002/adhm.202201975

[6] Cavender-Word, T.J. and D.A. Roberson, *Development of a Resilience Parameter for 3D-Printable Shape Memory Polymer Blends.* Materials, 2023. **16**(17): p. 5906. https://doi.org/10.3390/ma16175906

[7] Mehrpouya et al., *4D printing of shape memory polylactic acid (PLA).* Polymer, 2021. **230**: p. 124080. https://doi.org/10.1016/j.polymer.2021.124080

[8] García-Dominguez, A., J. Claver, and M.A. Sebastián, *Integration of additive manufacturing, parametric design, and optimization of parts obtained by fused deposition modeling (FDM). A methodological approach.* Polymers, 2020. **12**(9): p. 1993. https://doi.org/10.3390/polym12091993

[9] Ehrmann, G. and A. Ehrmann. *Shape-memory properties of 3D printed PLA structures.* in *Proceedings.* 2020. MDPI. https://doi.org/10.3390/CGPM2020-07198

[10] Ambati, S.S. and R. Ambatipudi, *Effect of infill density and infill pattern on the mechanical properties of 3D printed PLA parts.* Materials Today: Proceedings, 2022. **64**: p. 804-807. https://doi.org/10.1016/j.matpr.2022.05.312

[11] Wickramasinghe, S., T. Do, and P. Tran, *FDM-based 3D printing of polymer and associated composite: A review on mechanical properties, defects and treatments.* Polymers, 2020. **12**(7): p. 1529. https://doi.org/10.3390/polym12071529

[12] Villacres, J., D. Nobes, and C. Ayranci, *Additive manufacturing of shape memory polymers: effects of print orientation and infill percentage on shape memory recovery properties.* Rapid Prototyping Journal, 2020. **26**(9): p. 1593-1602. https://doi.org/10.1108/RPJ-09-2019-0239

[13] Liu et al., *4D printed anisotropic structures with tailored mechanical behaviors and shape memory effects.* Composites Science and Technology, 2020. **186**: p. 107935. https://doi.org/10.1016/j.compscitech.2019.107935

[14] Buj-Corral, I., A. Bagheri, and M. Sivatte-Adroer, *Effect of printing parameters on dimensional error, surface roughness and porosity of FFF printed parts with grid structure.* Polymers, 2021. **13**(8): p. 1213. https://doi.org/10.3390/polym13081213

[15] Rosales et al., *Characterization of shape memory polymer parts fabricated using material extrusion 3D printing technique.* Rapid Prototyping Journal, 2018. **25**(2): p. 322-331. https://doi.org/10.1108/RPJ-08-2017-0157

[16] Yao, T., et al., *Tensile failure strength and separation angle of FDM 3D printing PLA material: Experimental and theoretical analyses.* Composites Part B: Engineering, 2020. **188**: p. 107894. https://doi.org/10.1016/j.compositesb.2020.107894

[17] Singh, S. and R. Singh, *Mechanical characterization and comparison of additive manufactured ABS, Polyflex™ and ABS/Polyflex™ blended functional prototypes.* Rapid Prototyping Journal, 2020. **26**(2): p. 225-237. https://doi.org/10.1108/RPJ-11-2017-0234

[18] Chalgham, A., A. Ehrmann, and I. Wickenkamp, *Mechanical properties of FDM printed PLA parts before and after thermal treatment.* Polymers, 2021. **13**(8): p. 1239. https://doi.org/10.3390/polym13081239

[19] Peng et al., *Effects of FDM-3D printing parameters on mechanical properties and microstructure of CF/PEEK and GF/PEEK.* Chinese Journal of Aeronautics, 2021. **34**(9): p. 236-246. https://doi.org/10.1016/j.cja.2020.05.040

[20] Huang et al., *Study of processing parameters in fused deposition modeling based on mechanical properties of acrylonitrile-butadiene-styrene filament.* Polymer Engineering & Science, 2019. **59**(1): p. 120-128. https://doi.org/10.1002/pen.24875

[21] Liu, H., H. He, and B. Huang, *Favorable thermoresponsive shape memory effects of 3D printed poly (lactic acid)/poly (ε-caprolactone) blends fabricated by fused deposition modeling.* Macromolecular Materials and Engineering, 2020. **305**(11): p. 2000295. https://doi.org/10.1002/mame.202000295

[22] Bruère et al., *The influence of printing parameters on the mechanical properties of 3D printed TPU-based elastomers.* Progress in Additive Manufacturing, 2023. **8**(4): p. 693-701. https://doi.org/10.1007/s40964-023-00418-7

[23] Brancewicz-Steinmetz, E., J. Sawicki, and P. Byczkowska, *The influence of 3D printing parameters on adhesion between polylactic acid (PLA) and thermoplastic polyurethane (TPU).* Materials, 2021. **14**(21): p. 6464. https://doi.org/10.3390/ma14216464

[24] Contreras Raggio et al., *Height-to-Diameter Ratio and Porosity Strongly Influence Bulk Compressive Mechanical Properties of 3D-Printed Polymer Scaffolds.* Polymers, 2022. **14**(22): p. 5017. https://doi.org/10.3390/polym14225017

[25] Abdal-hay et al., *A review of protein adsorption and bioactivity characteristics of poly ε-caprolactone scaffolds in regenerative medicine.* European Polymer Journal, 2022. **162**: p. 110892. https://doi.org/10.1016/j.eurpolymj.2021.110892

[26] Liu et al., *Three-dimensional printing of poly (lactic acid) bio-based composites with sugarcane bagasse fiber: Effect of printing orientation on tensile performance.* Polymers for Advanced Technologies, 2019. **30**(4): p. 910-922. https://doi.org/10.1002/pat.4524

[27] Ursini, C. and L. Collini, *Fdm layering deposition effects on mechanical response of tpu lattice structures.* Materials, 2021. **14**(19): p. 5645. https://doi.org/10.3390/ma14195645.

[28] Le et al., *Optimizing 3D printing process parameters for the tensile strength of thermoplastic polyurethane plastic.* Journal of Materials Engineering and Performance, 2023: p. 1-12. https://doi.org/10.1007/s11665-023-07892-8

[29] Vidakis et al., *Strain rate sensitivity of polycarbonate and thermoplastic polyurethane for various 3d printing temperatures and layer heights.* Polymers, 2021. **13**(16): p. 2752. https://doi.org/10.3390/polym13162752

[30] Wang, P., B. Zou, and S. Ding, *Modeling of surface roughness based on heat transfer considering diffusion among deposition filaments for FDM 3D printing heat-resistant resin.* Applied Thermal Engineering, 2019. **161**: p. 114064. https://doi.org/10.1016/j.applthermaleng.2019.114064

[31] Pivar, M., D. Gregor-Svetec, and D. Muck, *Effect of printing process parameters on the shape transformation capability of 3D printed structures.* Polymers, 2021. **14**(1): p. 117. https://doi.org/10.3390/polym14010117

[32] Zhao et al., *Porous bone tissue scaffold concept based on shape memory PLA/Fe3O4.* Composites Science and Technology, 2021. **203**: p. 108563. https://doi.org/10.1016/j.compscitech.2020.108563

[33] Gibson, L.J. and M.F. Ashby, *Cellular Solids: Structure and Properties—Second Edition.* Published by the Press Syndicate of the University of Cambridge, 1997.

[34] De Vries, D., *Characterization of polymeric foams.* Eindhoven University of Technology, 2009. https://api.semanticscholar.org/CorpusID:10267107

[35] Nace et al., *A comparative analysis of the compression characteristics of a thermoplastic polyurethane 3D printed in four infill patterns for comfort applications.* Rapid Prototyping Journal, 2021. **27**(11): p. 24-36. https://doi.org/10.1108/RPJ-07-2020-0155

[36] Płatek et al., *Deformation process of 3D printed structures made from flexible material with different values of relative density.* Polymers, 2020. **12**(9): p. 2120. https://doi.org/10.3390/polym12092120

[37] Zhang et al., *Compression Behavior of 3D Printed Polymer TPU Cubic Lattice Structure.* Materials Research, 2022. **25**. https://doi.org/10.1590/1980-5373-MR-2022-0060

[38] Pazhamannil et al., *Investigations into the effect of thermal annealing on fused filament fabrication process.* Advances in Materials and Processing Technologies, 2022. **8**(sup2): p. 710-723. https://doi.org/10.1080/2374068X.2021.1946753

[39] Dave, H.K. and J.P. Davim, *Fused deposition modeling based 3D printing*. 2021: Springer. https://doi.org/10.1007/978-3-030-68024-4

[40] Ameen, A.A., A.M. Takhakh, and A. Abdal-hay, *An Overview of the Latest Research on the Impact of 3D Printing Parameters on Shape Memory Polymers.* European Polymer Journal, 2023: p. 112145. https://doi.org/10.1016/j.eurpolymj.2023.112145

[41] Farkas, A.Z., S.-V. Galatanu, and R. Nagib, *The Influence of Printing Layer Thickness and Orientation on the Mechanical Properties of DLP 3D-Printed Dental Resin.* Polymers, 2023. **15**(5): p. 1113. https://doi.org/10.3390/polym15051113

[42] Zeng et al., *Compression behavior and energy absorption of 3D printed continuous fiber reinforced composite honeycomb structures with shape*

memory effects. Additive Manufacturing, 2021. **38**: p. 101842. https://doi.org/10.1016/j.addma.2021.101842

[43] Zeng et al., *4D printed electro-induced continuous carbon fiber reinforced shape memory polymer composites with excellent bending resistance.* Composites Part B: Engineering, 2020. **194**: p. 108034. https://doi.org/10.1016/j.compositesb.2020.108034

[44] Abdal-hay et al., *Fabrication of biocompatible and bioabsorbable polycaprolactone/magnesium hydroxide 3D printed scaffolds: Degradation and in vitro osteoblasts interactions.* Composites Part B: Engineering, 2020. **197**: p. 108158. https://doi.org/10.1016/j.compositesb.2020.108158

[45] Sharma, R., R. Singh, and A. Batish, *On mechanical and surface properties of electro-active polymer matrix-based 3D printed functionally graded prototypes.* Journal of Thermoplastic Composite Materials, 2022. **35**(5): p. 615-630. https://doi.org/10.1177/0892705720907677

[46] Bartnikowski, M., et al., *A comprehensive study of acid and base treatment of 3D printed poly (ε-caprolactone) scaffolds to tailor surface characteristics.* Applied Surface Science, 2021. **555**: p. 149602. https://doi.org/10.1016/j.apsusc.2021.149602

[47] León-Calero, M., et al., *3D printing of thermoplastic elastomers: Role of the chemical composition and printing parameters in the production of parts with controlled energy absorption and damping capacity.* Polymers, 2021. **13**(20): p. 3551. https://doi.org/10.3390/polym13203551